Transient Response and Adjustment Timescales of Channel Width and Angle of Valley-Side Slopes to Accelerated Incision

Naoya Takahashi[1,*], J. Bruce H. Shyu[2,*], Shinji Toda[3], Yuki Matsushi[4], Ryoga Ohta[5], and Hiroyuki Matsuzaki[6]

[1] Department of Earth Science, Tohoku University, 6-3, Aramaki Aza-Aoba, Aoba-ku, Sendai 980-8578, Japan

[2] Department of Geosciences, National Taiwan University, No. 1, Sec. 4, Roosevelt Road, Taipei 106, Taiwan, ROC

[3] International Research Institute of Disaster Science (IRIDeS), Tohoku University, Aoba, 468-1, Aoba, Sendai 980-0845, Japan

[4] Disaster Prevention Research Institute, Kyoto University, Gokasho, Uji city, Kyoto 611-0011, Japan

[5] Faculty of Science and Engineering, Chuo University, 1-13-27, Kasuga, Bunkyo-ku, Tokyo 112-8551, Japan

[6] Micro Analysis Laboratory, Tandem Accelerator (MALT), The University Museum, The University of Tokyo, 2-11-16, Yayoi, Bunkyo-ku, Tokyo 113-0032, Japan

Corresponding author:

Naoya Takahashi (naoya.takahashi.c5@tohoku.ac.jp) (orcid.org/0000-0003-4196-1409)

J. Bruce H. Shyu (jbhs@ntu.edu.tw) (orcid.org/0000-0002-2564-3702)

Key Points:

- We use knickpoint travel time to estimate the time between knickpoint passage and channel/hillslope adjustments to accelerated incision.
- The adjustment of channel width after the passage of a knickpoint takes 2–5 times longer than the adjustment of valley-side slope.
- Adjustment of the entire river basin takes much longer than the time a knickpoint takes to travel upstream to the channel heads.

Abstract

Studying bedrock rivers during their transient states helps understand the response of a fluvial system to changed boundary conditions. Although studies show how river form adjusts to changes in incision or rock uplift rates, field constraints on the timescale of this adjustment are limited. We present a method that uses knickpoint travel time to estimate the adjustment times of channel width and angle of valley-side slopes to accelerated incision. The travel time of knickpoints between their current positions and the points where changes in width or hillslope angle have just finished represents the time required for morphological adjustment after knickpoint passage. We documented channel slopes, channel widths, and hillslope angles along six rivers that cross an active normal fault in Iwaki, Japan, and identified river sections in a transient state. Channel slopes and basin-averaged erosion rates determined from ^{10}Be concentrations are distinct between rivers near and distant from the fault, suggesting that past increases in fault throw rates triggered the knickpoint formation and the observed transient response. Adjustment time depends on the slope exponent in the detachment-limited model and is 2–5 times greater for channel width than hillslope angle, indicating that catchment adjustment times can be much longer than times predicted only by knickpoint travel time. The fact that channel slope, channel width, and hillslope angle have distinct adjustment times underlines the importance of correctly identifying river sections that are fully adjusted to the new boundary conditions when inferring erosion or relative uplift rates for bedrock rivers.

Plain Language Summary

Bedrock rivers adjust their forms in response to changes in their boundary conditions, such as underlying rock types, climate, and tectonics, which means that establishing their quantitative relationships between these boundary conditions may enable us to infer rates of erosion or relative uplift from river morphologies. Although it is well known how river and hillslope forms adjust after an increase in erosion rates, the timescale of these adjustments is difficult to constrain in an actual landscape. This study presents a method to estimate the adjustment times of channel width and hillside slope angles along the sides of a valley. We studied a set of rivers that cross an active normal fault and documented the variations of channel and hillslope forms along their courses. These rivers are now changing their shapes after motion on the fault has

increased their erosion rates. Our analysis shows that channel width likely takes 2–5 times longer to complete its adjustment than does the hillslope angle. Our findings show that channel slope, channel width, and hillslope angle all have distinct adjustment times. It may take longer than previously thought for an entire river system to adjust to new boundary conditions.

1. Introduction

Because the incision of rivers into bedrock is a major element in the formation of mountain landscapes, quantifying incision rates and their relationships with external forces is important for understanding landscape evolution. The morphology of channels and hillslopes is closely related to erosion rates, and a long history of research has gone into establishing their functional relationships (e.g., Ahnert, 1970; Wobus et al., 2006a; Roering et al., 2007; Kirby & Whipple, 2012). A sudden increase in the rate of base-level fall (i.e., relative uplift) can enhance local incision rates and may generate a knickpoint that migrates upstream (e.g., Whipple & Tucker, 1999; Crosby & Whipple, 2006). As it does so, channels and hillslopes along its passage gradually adjust their forms to the accelerated incision rates. Knickpoints are common in tectonically active areas, and thus knowledge of the transient response of rivers to an increase in incision rates may enable researchers to infer a region's erosional or tectonic history from river morphologies.

Channel slope, channel width, and the angle of valley-side slopes are closely related to channel incision rates, and many studies have focused on quantifying relationships between morphologies of channel and hillslope and rates of incision or relative uplift (e.g., Whipple & Tucker, 1999; Snyder et al., 2000; Lavé & Avouac, 2001; Roering et al., 2001; Montgomery & Brandon, 2002; Reinhardt et al., 2007; Yanites & Tucker, 2010). The channel steepness index, expressing the channel slope normalized by upstream drainage area (e.g., Snyder et al., 2000), increases after the passage of a knickpoint in response to an increase in incision rates. Channel steepness downstream from the migrating knickpoint is assumed to reach a new steady-state value and is often positively correlated with uplift rates (e.g., Kirby & Whipple, 2012; Regalla et al., 2013; Chen et al., 2015; Gallen & Wegmann, 2017). Channel width can become wider or narrower in response to increased incision rates or be insensitive to incision rates (e.g., Lavé & Avouac, 2001; Snyder et al., 2003; Yanites & Tucker, 2010). According to a numerical study that considered the effects of sediment cover, channel narrowing occurs after the knickpoint passage, but as the knickpoint travels upstream the local sediment supply continues to increase, resulting in gradual widening of the channel (Yanites, 2018). A similar width adjustment was observed in a flume experiment (Baynes et al., 2022). Hillslope morphology is set by river incision at its base. The hillslope angle increases with incision rates until it reaches a threshold angle, above which it becomes insensitive to incision rate (e.g., Montgomery & Brandon, 2002). The threshold angle, usually ~30°–40°, is reached at relatively slow incision rates of 0.2–1.0 mm/yr (e.g., Montgomery & Brandon, 2002; Ouimet et al., 2009; DiBiase et al., 2012).

Whereas many studies have examined how river morphologies adjust to changes in incision rates, relatively few have attempted to quantify the adjustment timescales of channels and hillslopes to accelerated incision. Such studies require a chronology that specifies the times at which these morphological adjustments begin and end. However, in actual landscapes, it is very difficult to constrain those timings except for channel slope (e.g., Crosby & Whipple, 2006; Whittaker & Boulton, 2012). The arrival of a knickpoint triggers a change in channel slope from which a rate of knickpoint retreat can be calculated (e.g., Whipple & Tucker, 1999; Royden & Perron, 2013). Therefore, when the time and place a knickpoint is generated are known, the timescale of channel slope adjustment can be estimated based on the knickpoint's travel distance and travel speed (e.g., DiBiase et al., 2015).

The adjustment timescales of channel width and hillslope, unlike that for channel slope, are difficult to estimate by using field evidence. Instead, they have been studied by numerical modeling (e.g., Roering et al., 2001; Mudd & Furbish, 2007; Yanites, 2018; Turowski, 2020). Yanites (2018), modeling the evolution of channel width after knickpoint passage, showed that the full adjustment could take 10^5–10^6 years. Roering et al. (2001) used sediment transport models on hillslopes to estimate the adjustment time of valley-side slopes to a change in base-level lowering rates. The model parameters used in these studies were based on field observations. However, we still know little about the actual adjustment timescales of channel width and hillslopes, due to the difficulties in constraining when those adjustments started and finished.

This paper presents a method to quantify the adjustment timescales of channel width and the angle of valley-side slopes. We applied the method to bedrock rivers that cross an active normal fault near the city of Iwaki, Japan. Because changes in channel width and hillslope follow the passage of a knickpoint, we can use knickpoint travel times to estimate three quantities at any given location: response time, the time between the start and finish of a morphological adjustment; delay time, the lag time between the knickpoint arrival and the start of morphological adjustment; and adjustment timescale, the sum of response and delay times, representing the time between knickpoint passage and the finish of adjustment. Therefore, for the adjustment of channel slopes, the delay time at a given location is always zero, the response time is the time from the knickpoint passage until the channel slope attains a steady-state value, and the adjustment time equals the response time. We investigated channel slope, channel width, and hillslope angle along trunk streams and identified points at which morphological adjustments started and finished. Because we cannot know exactly when channel or hillslope adjustments have finished, we defined the end of adjustment as the condition where channel and hillslope forms are indistinguishable from those presumably at a steady state. We then calculated knickpoint travel times and estimated the response and delay times of channel width and hillslope angle. We use these results to discuss how the channel width and the angle of valley-side slopes change following an increase in channel incision rates, highlighting the need to inspect channels and hillslopes along a trunk stream and its tributaries when inferring incision or tectonic histories from river morphologies.

2. Background

2.1 Tectonic and Geologic Background

Iwaki is in the Tohoku region of northeastern Japan, which is subjected to E-W compression due to westward subduction of the Pacific plate under the Eurasia plate (Figure 1a). Although most earthquakes in Tohoku are characterized by reverse faulting, analysis of microearthquakes during 2003–2010 has revealed that the Iwaki area has been in an extensional stress regime since before the 11 March 2011 Mw 9.0 Tohoku-Oki earthquake (Imanishi et al., 2012). Shortly after the Tohoku-Oki event, a normal-faulting event of Mw 6.6 occurred in Iwaki on 11 April 2011. This earthquake produced surface ruptures along the Yunodake and Itozawa faults (Figure 1a) (e.g., Fukushima et al., 2013; Toda & Tsutsumi, 2013). The Yunodake and Itozawa faults are normal faults dipping SW and WSW, respectively, that form a half-graben between them (Mitsui, 1971), suggesting that this area has experienced extension on a geological timescale. The vertical slip rate of the Yunodake fault is unknown. A paleoseismic trenching study (Miyashita, 2018) showed that three surface-rupturing earthquakes including the 2011 event occurred on the Yunodake fault within the last 7 ky. If we assume that each of these produced vertical displacements similar to that in 2011 (~80 cm: Toda & Tsutsumi, 2013), a rough estimate of the fault throw rate is ~0.34 mm/yr.

Bedrock around the Yunodake fault consists of metamorphic and granitic rocks of Cretaceous age and sedimentary rocks of Miocene age (e.g., Kubo et al., 2007) (Figure 1b). Cretaceous metamorphic rocks include siliceous, mafic, pelitic and calcareous rocks (Kano et al., 1973; Hiroi et al., 1987; Kubo et al., 2007). Cretaceous granodiorite and porphyritic granodiorite occur along the middle and eastern part of the Yunodake fault (Kubo et al., 2007). Miocene sedimentary rocks southwest of the Yunodake fault include marine and nonmarine clastic rocks (Kubo et al., 2007) that overlie Cretaceous metamorphic rocks (Mitsui, 1971).

We focus on six trunk streams, numbered 1 through 6, along the Yunodake fault (Figure 1). Their drainage areas range from 1.6 to 24.1 km^2 and average 7.4 km^2 (Table S1). The substrates are either metamorphic or granitic rocks. Riverbeds are typically covered with gravel in reaches of metamorphic rocks and with sand in reaches of granitic rocks. Although Basins 2–6 intersect with or are very close to the fault, Basin 1 does not cross the fault. Basins 2–6 are characterized by steeper downstream reaches and gentler upstream reaches of smaller relief (Figure 1c).

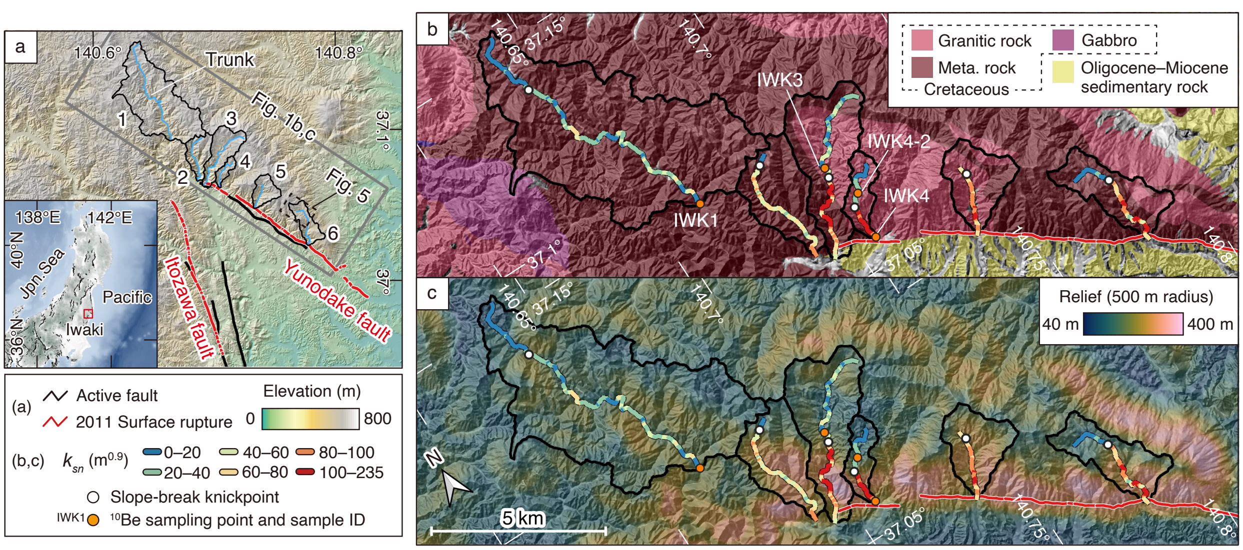

Figure 1. (a) Location and topography of the study area. Drainage basins and their trunk streams are labeled with their identification number (1–6). The inset map shows topography and active fault traces in eastern Japan. Active fault traces are from Nakata and Imaizumi (2002). Surface rupture traces are after Toda and Tsutsumi (2013). (b) Geologic map around the Yunodake fault (Kubo et al., 2007; Geological Survey of Japan, 2020). (c) Topographic relief in the area of (b) within circular windows of 500 m radius.

2.2. Channel and Hillslope Morphology

2.2.1. Channel Slope

In a stream at steady state, local channel slope (S) is a function of flow discharge, which is commonly represented by upstream drainage area (A):

$$S = k_s A^{-\theta}, \tag{1}$$

where k_s is a steepness index and θ is a concavity index (e.g., Flint, 1974; Snyder et al., 2000). Equation (1) holds only above a critical drainage area ($A > A_{\mathrm{crt}}$), at which the dominant erosional process changes from colluvial (debris flows) to fluvial processes (e.g., Montgomery & Foufoula-Georgiou, 1993; Stock & Dietrich, 2003). In drainage areas smaller than A_{crt}, channel slope either increases with or is independent of drainage area. The concavity index typically ranges between 0.4 and 0.6 (e.g., Kirby & Whipple, 2012).

The standard stream power model (e.g., Howard & Kerby, 1983) predicts a relation between channel slope and upstream drainage area similar to equation (1):

$$S = (E/K)^{1/n} A^{-m/n}, \tag{2}$$

where E is a local erosion rate, K is erodibility, m is related to the dominant erosion process and n is related to the hydraulic scaling relationships among channel width, flow discharge, and drainage area (e.g., Whipple & Tucker, 1999). From equations (1) and (2), under a steady state where local erosion rates match local uplift rates (U), channel steepness can be written as

$$k_s = (E/K)^{1/n} = (U/K)^{1/n}. \tag{3}$$

Because the concavity index is independent of uplift rates when the gradient of local uplift rates within a basin has a negligible impact on a channel profile (e.g., Snyder et al., 2000), a fixed concavity index ($\theta = \theta_{ref}$, equation (1)) is used to calculate k_s, and the resulting channel steepness is termed a normalized steepness index (k_{sn}; Wobus et al., 2006a).

A sustained increase in the rate of base-level lowering can generate a knickpoint (or a knickzone). This knickpoint propagates upstream and separates the longitudinal river profile into two segments: an adjusted segment downstream with higher steepness and a pre-adjusted segment upstream with lower steepness. This mobile knickpoint, called a slope-break knickpoint (e.g., Whipple et al., 2013), is readily distinguished from a stationary knickpoint (vertical-step knickpoint) that has different origins, such as a local decrease in bed erodibility associated with resistant substrates.

2.2.2. Channel Width

The channel width (W) of bedrock rivers is a power function of drainage area (e.g., Montgomery & Gran, 2001):

$$W = k_w A^b, \tag{4}$$

where k_w (unit: m$^{1\text{-}2b}$) is a wideness index (e.g., Allen et al., 2013) and b is a positive exponent that is typically 0.3–0.5 at a steady state (e.g., Whipple, 2004). A larger wideness index indicates a wider channel. Similar to k_{sn} and θ_{ref}, k_w calculated using a fixed value of b (b_{ref}) is a normalized wideness index (k_{wn}). An adjustment in channel width in response to accelerated incision should appear as a break in the hydraulic scaling of equation (4) or a change in average k_{wn} values with distance along the stream.

2.2.3. Angle of Valley-Side Slopes

In mountainous landscapes, drainage basins consist primarily of hillslopes, and material transport on hillslopes dictates the sediment supply to channels (e.g., Roering, 2008). Following the passage of a knickpoint produced by increased base-level lowering rates, hillslopes become steeper such that hillslope lowering keeps pace with channel incision (e.g., Roering et al., 2001). A downstream increase in hillslope angle is expected downstream of a slope-break knickpoint, and our analysis focused on this transition.

2.3. Knickpoint Travel Speed and the Timescales of Channel Width and Hillslope Angle Adjustments

Following the passage of a slope-break knickpoint, the channel width and the angle of valley-side slopes are expected to change until the local incision rate matches the local uplift rate. This morphological adjustment is characterized by a response time and a delay time, as defined in section 1. We estimated the response and delay times for channel width and hillslope angle based on knickpoint travel time.

Figure 2 schematically illustrates the response of a valley-side slope to accelerated incision. Hillslopes downstream from the knickpoint can be divided into three sections representing the phases of morphological adjustment. The pre-adjustment hillslope extends from upstream to slightly downstream of the knickpoint, and its angle reflects the incision rate before acceleration. The adjusted hillslope, well downstream from the knickpoint, has an angle that is fully adjusted to the accelerated incision. Between these two sections is the adjusting hillslope, with an angle that is currently changing in response to the accelerated incision. Because the knickpoint propagates upstream, its travel time from the boundary between the pre-adjustment and adjusting sections to the current knickpoint position represents the delay time. The knickpoint travel time from this boundary to the boundary between the adjusting and adjusted sections is the response time. The adjustment time is the sum of the response and delay times.

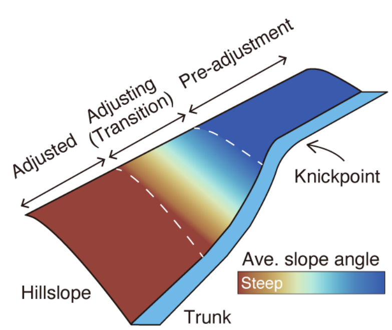

Figure 2. Schematic diagram of the right bank of a stream showing the response of hillslope angle to accelerated incision. The hillslope angle starts to change at the boundary between the pre-adjustment and adjusting sections and finishes at the boundary between the adjusting and adjusted sections.

Following a sustained increase in incision rates, knickpoint travel distance in χ-space is written as (Royden & Perron, 2013; Mitchell & Yanites, 2019):

$$\chi_{kp}(t) = \begin{cases} \dfrac{nU_{ini}}{\left(\frac{U_{ini}}{K}\right)^{\frac{1}{n}} A_0^{-\frac{m}{n}}} t & n < 1 \quad (5a) \\ KA_0^{\frac{m}{n}} t & n = 1 \quad (5b) \\ \dfrac{U_{fin} - U_{ini}}{\left(\left(\frac{U_{fin}}{K}\right)^{\frac{1}{n}} - \left(\frac{U_{ini}}{K}\right)^{\frac{1}{n}}\right) A_0^{-\frac{m}{n}}} t & n > 1 \quad (5c) \end{cases}$$

where $\chi_{kp}(t)$ is a χ of a mobile knickpoint at time t since knickpoint generation. A_0 is a reference drainage area, which was set at 1 in this study. Subscripts ini and fin represent the initial and final steady state, respectively; thus U_{ini} and U_{fin} are initial and final uplift rates ($U_{ini} < U_{fin}$). Substituting equation (3) for equation (5) and solving equation (5) with respect to t, the knickpoint travel time since the incision rate increase (t = 0) is

$$t = \begin{cases} \dfrac{k_{sn\ ini}}{nU_{ini}} \chi_{kp}(t) & n < 1 \quad (6a) \\ \dfrac{1}{K} \chi_{kp}(t) & n = 1 \quad (6b) \\ \dfrac{k_{sn\ fin} - k_{sn\ ini}}{U_{fin} - U_{ini}} \chi_{kp}(t) & n > 1. \quad (6c) \end{cases}$$

2.4. Basin-Averaged Erosion Rate Determined from Cosmogenic ^{10}Be Concentration

The ^{10}Be concentration in fluvial sediment ($\bar{C}$: atoms/g) is used to estimate the average erosion rate within a catchment ($\bar{D}$: g/m^2 yr) (e.g., Brown et al., 1995a; Bierman & Steig, 1996; Granger et al., 1996) by

$$\bar{D} = P_0 \Lambda / \bar{C}, \tag{7}$$

where P_0 (atoms/g yr) is the cosmogenic ^{10}Be production rate at the surface and Λ (g/cm^2) is the attenuation length of particles responsible for ^{10}Be production. Because the total sediment mass produced in a catchment is the sum of the sediment from its nested sub-catchments, average erosion rates within and outside the sub-catchments can be estimated by analyzing ^{10}Be samples from multiple sites in the catchment (e.g., Regalla et al., 2013):

$$\bar{D} = \sum_{i=1}^{j} D_i A_i \,/ \sum_{i=1}^{j} A_i\,, \tag{8}$$

where D_i and A_i are the average erosion rate and drainage area of sub-catchment i, respectively, and j is the number of subcatchments.

3. Method

3.1. Observations of Channel and Hillslope Morphology

We compiled observations of the along-trunk variations of channel slope, channel width, and hillslope angle as detailed below. We used the channel slope data to identify the current knickpoint position, and we used the other observations to determine the points where the adjustments of channel width and hillslope angle started and finished.

3.1.1. Normalized Steepness Index

We analyzed a digital elevation model (DEM) of the study area to calculate the normalized steepness index k_{sn} every 50 m along trunk streams using Topotoolbox 2 (Schwanghart & Scherler, 2014). The DEM, obtained from the Geospatial Information Authority of Japan, has a resolution of 10 m. We first determined A_{crt} and then calculated k_{sn} for channel reaches with $A > A_{crt}$. We also calculated χ (Perron & Royden, 2013) and constructed χ-elevation (z) plots (χ-plots):

$$\chi = \int_{x_b}^{x} (A_0/A(x))^{\frac{m}{n}}\, dx \tag{9}$$

$$z(x) = z(x_b) + (E/KA_0^m)^{\frac{1}{n}} \chi \tag{10}$$

where x is the distance along a stream course measured from the outlet of the channel reach, x_b is the distance at the outlet (thus $x_b = 0$). Equation (10) is the integral form of equation (2) under the assumption of a spatially uniform E and K, and it predicts that the slope of a χ-plot represents a reach-averaged value of k_{sn}. A knickpoint appears as a kink in a χ-plot. We used the k_{sn} values and χ-plots to determine the current positions of slope-break knickpoints (at the upstream end of knickzones), where the adjustment of channel slope begins.

3.1.2. Field Measurement of Channel Width

We measured bankfull channel widths in the field every 30–100 m along trunk streams using a laser rangefinder (TruPulse 360B Laser Technology). Measurement error is approximately ±30 cm. Width measurements depend on how one defines flow depth at bankfull stage. The bankfull depth is typically identified based on the limits of active abrasion, vegetation boundaries, and remnants of flood debris (e.g., Whittaker et al., 2007). Where there were multiple candidates for the high-flow depth, we measured channel widths at each candidate level and calculated their average. The measured width of each trunk river was fitted to equation (4) to estimate exponent b based on least squares. We determined b_{ref} by averaging b of all river segments whose width variations were consistent with the general scaling of equation (4). We then used the resulting b_{ref} values and upstream drainage areas calculated from the 10 m DEM to calculate the normalized wideness index k_{wn}.

3.1.3. Average Angle of Valley-Side Slopes

We calculated the angles of hillslopes adjacent to trunk streams using the 5 m DEM provided by the Geospatial Information Authority of Japan. We used this high-resolution DEM because the accuracy of hillslope angles depends on the DEM grid size. Because the available 5 m DEM lacks data along the streams, we could not use it for the channel analysis. We mapped hillslopes along trunk streams based on the upstream drainage area, slope aspect, and slope curvature. We did not include hillslopes along tributaries with drainage areas greater than A_{crt} as our focus was on trunk streams. Although it was difficult to determine a clear threshold, we also excluded hillslopes along small tributaries (maximum area < A_{crt}) visible on the 5 m DEM (Figure S1). We then segmented mapped valley-side slopes every 50 m along trunk streams and calculated average angles for each hillslope segment.

3.1.4. Identifying Sections of Transient Response

To identify river sections where hillslopes and channels are undergoing transient response to a knickpoint passage, we calculated 8-point moving averages of k_{wn} and hillslope angle. Given the large natural variability in channel width and hillslope angle, we augmented the moving averages with statistical tests to identify the sections in transience. The Kolmogorov-

Smirnov test showed that in Basin 1, k_{wn} values were normally distributed (p = 0.64) and hillslope angles were not normally distributed (p << 0.01) at the 5% significance level. Therefore, we applied the Student's *t* test for k_{wn} data and the Mann-Whitney U test for hillslope angle data. In these tests, we used 16 contiguous samples and determined whether the difference between the upstream 8 samples and the downstream 8 samples was statistically significant. Despite trying various significance levels, we could not properly identify sections experiencing transient response. Therefore, we defined transient sections as those where the moving average values showed a gradual decrease or increase and where the p-value of statistical tests was smaller than those of adjacent channel sections.

3.2. Adjustment Timescales of Channel Width and Hillslope Angle

Using equation (6), we calculated knickpoint travel time for n values of 2/3, 1, and 5/3 (e.g., Whipple et al., 2000) and estimated the delay, response, and adjustment times of channel width and valley-side slope angles in response to a sustained increase in incision rates. Normalized channel steepness at the initial and final steady state were defined as the average k_{sn} upstream and downstream of a slope-break knickpoint, respectively. We assumed that the erodibility constant (K) was uniform over time and calculated K using k_{sn} and ^{10}Be-derived erosion rates with equation (3).

3.3. Basin-Averaged Erosion Rate Determined from Cosmogenic ^{10}Be Concentration

We collected four sand samples (diameter < 2 mm) from trunk streams and measured ^{10}Be concentrations of quartz grains to determine basin-averaged erosion rates (Figures 1 and S2). We purified quartz following a method adapted from Kohl and Nishiizumi (1992). We first crushed and sieved samples to obtain grains 0.25–1 mm in diameter. These were heated in 9% HCl to remove carbonates, iron oxides, and organic materials, then quartz was separated from the samples using sodium polytungstate. The extracted quartz was leached using a 1% HF and HNO_3 solution to remove residual feldspars and meteoric ^{10}Be. Then, after adding a ^{9}Be spike, the quartz was dissolved with HF, HNO_3, and $HClO_4$. After the solution was used in anion- and cation-exchange chromatography, NH_4OH was added, and the precipitant was heated to obtain

BeO. $^{10}Be/^{9}Be$ ratios were measured using accelerator mass spectrometry at Micro Analysis Laboratory, Tandem Accelerator, the University of Tokyo (Matsuzaki et al., 2007).

^{10}Be production rates were calculated using scaling factors presented in Stone (2000). We computed topographic shielding factors for all sampled points using the 10 m DEM and an algorithm developed by Li (2013). Attenuation lengths for neutrons, slow muons and fast muons were set at 160, 1500, and 5300 g/cm^2, respectively (Brown et al., 1995b; Gosse & Phillips, 2001; Braucher et al., 2003). Contributions of slow and fast muons to the total ^{10}Be production at the surface were assumed to be 1.2% and 0.65%, respectively (Braucher et al., 2003). We assumed a bulk density of 1.63 g/cm^3 for the shallow subsurface materials on hillslopes (Nakamura et al., 2014). Although it sometimes snows in Iwaki, we did not consider the effect of snow shielding on ^{10}Be production because the snow cover was mostly less than several centimeters deep during 1960–2008 (Japan Meteorological Agency, 2021).

4. Results

4.1. Channel and Hillslope Morphology

4.1.1. Steepness of Stream Channels

Calculated values of normalized channel steepness (k_{sn}) are summarized in Figure 3. Each of the six drainage basins contains a slope-break knickpoint dividing the trunk streams into a downstream segment with greater k_{sn} and an upstream segment with smaller k_{sn} (Figures 1 and 3). Downstream segments of Basins 2–6 are much steeper than that of Basin 1, suggesting that incision rates in Basin 1 are much slower than in other basins. The channel steepness in the downstream segment of Basin 1 is three times greater than that of the upstream segment (Figure 3), suggesting that Basin 1 may be at a transient state. However, because the trunk stream of Basin 1 does not cross the Yunodake fault and we cannot know where the knickpoint formed, we will not discuss its morphological characteristics in detail. A slope-break knickpoint in Basin 3 occurs near a boundary between granitic rocks and schist (Figure 1), presenting the possibility that differential rock erodibility may explain the observed increase in k_{sn}. However, channel steepness does not change significantly at similar lithologic boundaries in Basins 3 and 4

(Figures 1b and S2). Therefore, we assumed that factors other than differential rock erodibility contributed to the formation of the knickpoint in Basin 3.

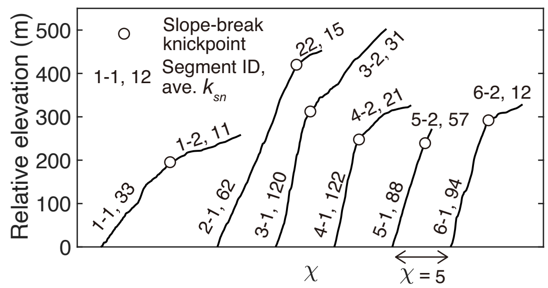

Figure 3. A χ-plot for the trunk streams in Basins 1 to 6. Relative elevation (y-axis) denotes the elevation above the basin outlet.

4.1.2. Channel Width

We measured channel width and depth at 308 points, which are presented in the supporting information (Table S2). Channel width in Basins 1, 2, and 4 increases monotonically with drainage area and follows the general hydraulic scaling of equation (4) (Figure 4; Table 1). Normalized wideness index (k_{wn}, b_{ref} = 0.42) in Basins 1, 2, and 4 do not vary significantly over their entire reaches (Figure 4). It is noteworthy that k_{wn} for the trunk streams of Basins 1 and 2 are identical despite their twofold difference in k_{sn}. This result implies that their channel widths are insensitive to changes in channel incision rates or that they have not started to adjust to the accelerated incision (e.g., Snyder et al., 2003; Zhang et al., 2017).

While channel width increases with drainage area in upstream segments of Basins 3 and 5, in their downstream segments channel width decreases or does not change significantly with increasing drainage area (Figure 4). In Basin 3, channel width starts to decrease at A = ~5.2 km^2, and that transition occurs near the lithologic boundary between granitoids and metamorphic rocks (Figures 4e and 4f). These results suggest that substrate property may partly control channel width. However, the break in the scaling relationship for channel width observed in Basin 3 cannot be solely attributed to the difference in substrates because the channel width continues to decrease downstream from the lithologic boundary (Figure 4e and 4f).

In Basin 6, the channel width changes by a factor of 2 at A = 1.5 km^2 (Figure 4k and 4l) and clearly deviates from the general trend of equation (4). Downstream from this point, bedrock extensively crops out in the riverbed and channel width decreases with drainage area, which is likely associated with accelerated river incision as in Basins 3 and 5. The upstream reaches are covered by thick alluvium. Aerial photographs taken in 1976 and 1986 show that many trees upstream in Basin 6 were cut during this period and the surrounding areas were widely excavated (Figure 5). This human activity displaced large amounts of soil, which currently occupies the channel and results in channel narrowing upstream of the knickpoint.

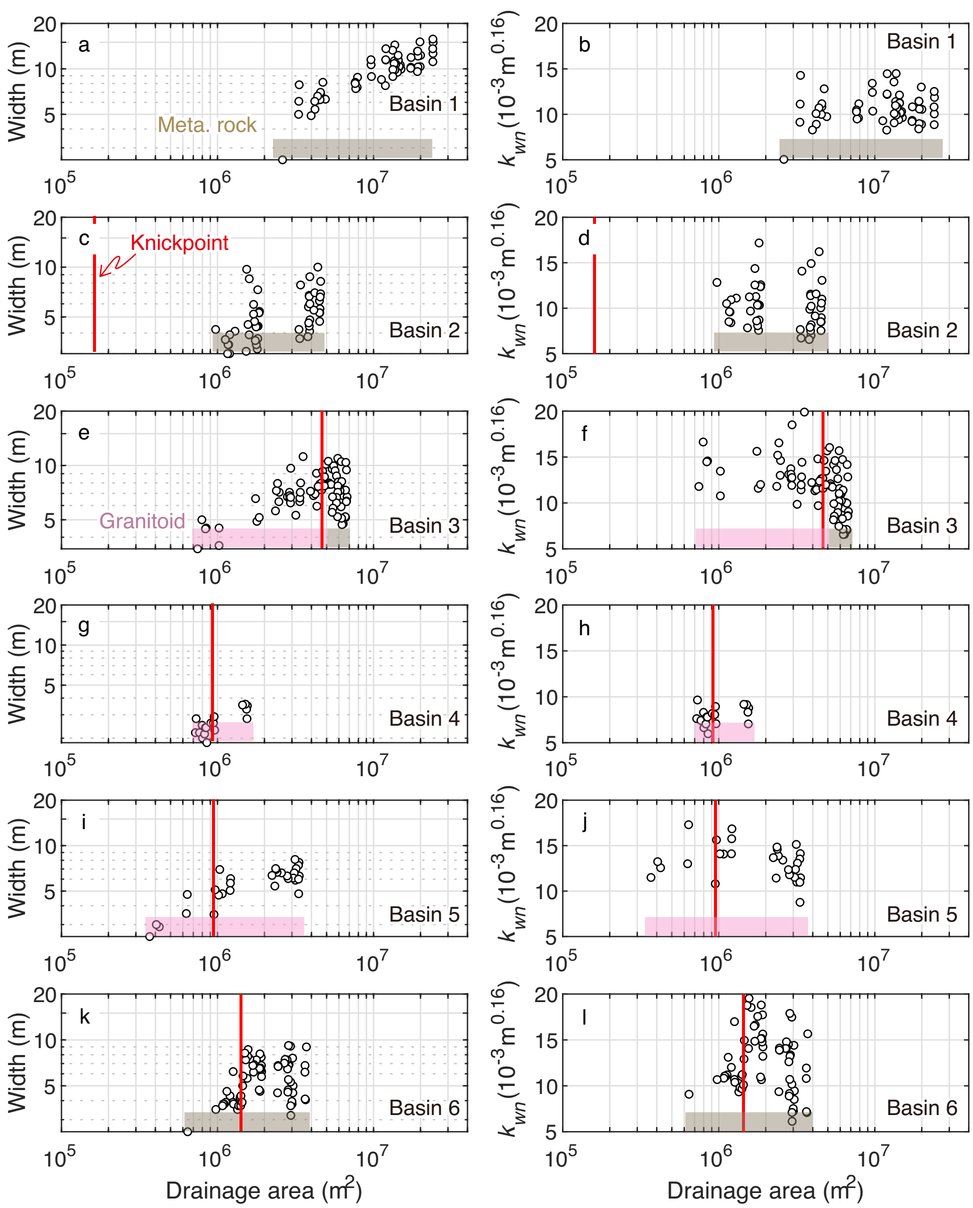

Figure 4. (Left) Channel width versus drainage area for the trunk streams. (Right) Normalized channel wideness (b_{ref} = 0.42) versus drainage area. Colored bars at the bottom of each diagram indicate substrate rock types in the corresponding river sections. Red vertical lines indicate positions of slope-break knickpoints.

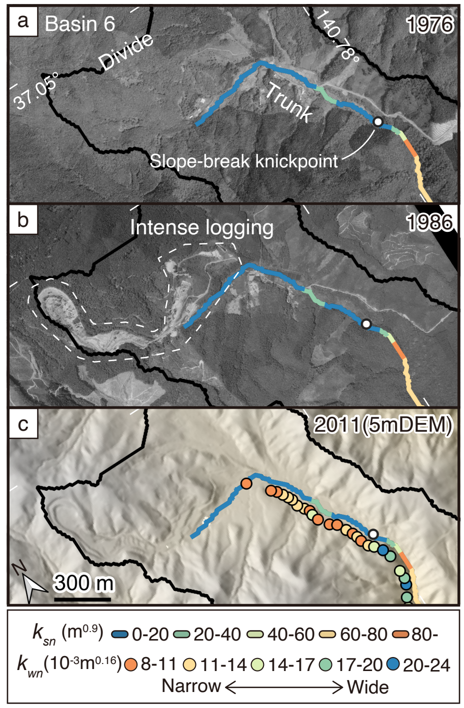

Figure 5. Deforestation in the headwater area of Basin 6. (a, b) Aerial photographs taken in 1976 and 1986, respectively. (c) Relief map created from the 5 m DEM issued in 2011 by the Geospatial Information Authority of Japan. Colored points along the trunk stream show normalized channel wideness at nearby sites.

Table 1
Results of Field Measurement and Regression of Channel Width

Basin/ segment	Max. area (km^2)	Min. area (km^2)	k_w	b^*	R^2	Ave k_{wn} (10^{-3} $m^{0.16}$)
1	24.1	0.025	3.45	*0.43*	0.73	10.6
2	4.6	0.021	3.43	*0.40*	0.41	10.2
3	6.9	0.021	5.37	0.20	0.20	12.0
3-downstream	6.9	6.2	2.52	0.52	0.03	9.2
3-upstream	5.4	0.021	4.70	*0.35*	0.51	13.2
4	1.6	0.1	2.69	*0.52*	0.73	8.1
5	3.4	0.4	4.75	0.30	0.64	13.4

5-downstream	3.4	2.8	5.28	0.18	0.00	12.1
5-upstream	2.4	0.4	4.79	*0.39*	0.65	14.3
6	3.8	0.3	4.73	0.26	0.13	12.8
6-downstream	3.8	1.7	7.19	−0.17	0.03	12.6
6-upstream	1.6	0.3	2.96	1.77	0.53	12.7

*Numbers in italics were used to calculate b_{ref}.

4.1.3. Angle of Valley-side Slopes

As illustrated in Figure 2, hillslopes in Basins 1–6 consist of three sections: an upstream section with gentler slopes, a downstream section with steeper slopes, and an intervening transition section. Hillslope angles in the upstream sections were positively correlated with normalized channel steepness (Figure 6). In the downstream sections, hillslope angles were less sensitive to channel steepness and clustered at 35°–38°, suggesting that these are predominantly threshold hillslopes (e.g., Ouimet et al., 2009). Left-skewed distributions of hillslope angles also support the interpretation that the downstream sections have threshold hillslopes (Figure 6b) (DiBiase et al., 2012). These transitions from gentler to steeper hillslopes occur downstream of the knickpoints and presumably result from the change in incision rates. Also, it is worth noting that the histograms for hillslope angles along the trunk stream distinctly differ from those for the whole basin (Figure 6b and 6c).

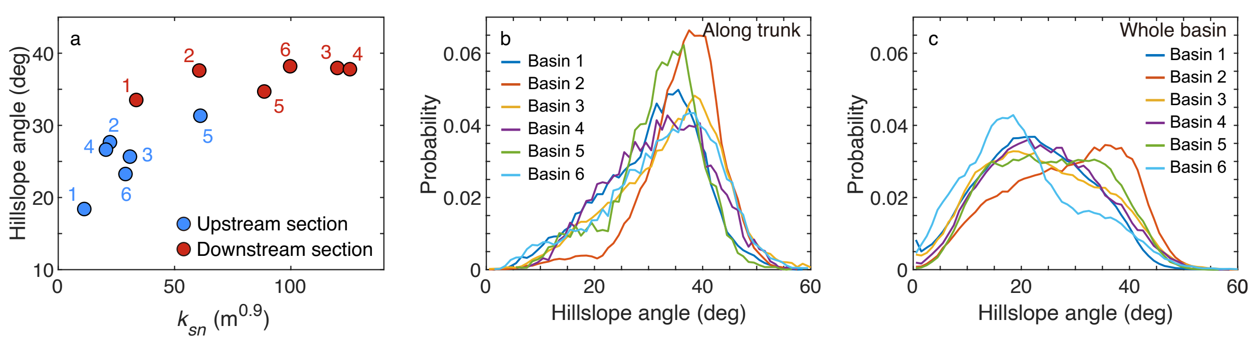

Figure 6. (a) Hillslope angle versus normalized channel steepness for upstream and downstream segments of the six basins. (b) Histogram of hillslope angles along trunk streams. (c) Histogram of hillslope angles in each entire basin. The bins in (b) and (c) are 1° wide.

4.1.4. Identifying Sections undergoing Transient Response

We used the moving averages of channel and hillslope parameters and the *p*-values from statistical tests to identify river sections experiencing transient response to accelerated incision. Figure 7 shows the along-trunk variations of channel and hillslope morphology in Basin 3, and those for the other basins are shown in Figure S5. As mentioned in section 4.1.1, we excluded Basin 1 from further analysis because its trunk stream does not cross the Yunodake fault. Also, we do not discuss hillslope adjustment time for Basin 5 because the observed increase in hillslope angle starts upstream of the knickpoint.

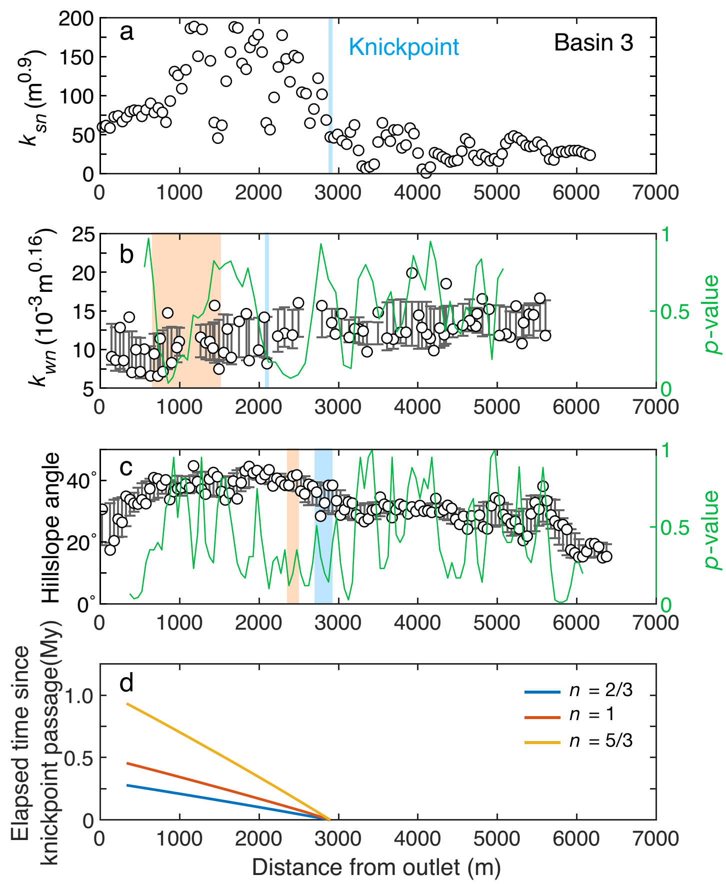

Figure 7. Variations of channel width and hillslope morphology along the trunk stream in Basin 3. (a) Normalized channel steepness (k_{sn}). The blue line indicates the current knickpoint position. (b) Normalized channel wideness (k_{wn}). The green line indicates the *p*-value from Student's *t* test. (c) Average hillslope angle in each 50 m segment of the trunk stream. The green line indicates the *p*-value from the Mann-Whitney U test. Gray bars in (b) and (c) represent standard deviation of 8-point moving averages and blue and orange areas indicate sections where

adjustments start and finish, respectively. (d) Time elapsed since knickpoint passage (knickpoint travel time) for three different values of n.

4.2. Substrate Erodibility Calculated from Basin-Averaged Erosion Rates

The basin-averaged erosion rates of our study basins ranged between 260 and 400 g/m^{2}yr, equivalent to 0.16–0.25 mm/yr (Table 2). Basin 4 differs from the others in consisting almost entirely of granitic rock. It also lacks evidence of recent large slope failures, which dilute the average ^{10}Be concentration of fluvial sand downstream by supplying material with low ^{10}Be concentrations. Thus, we used equation (8) to calculate the basin-averaged erosion rate of the downstream half of Basin 4 (IWK4-1, Table 2) and found that it is faster than that of the upstream half of Basin 4 (IWK4-2, Table 2). Overall, basin-averaged erosion rates were positively correlated with average k_{sn} (Table 2, Figure S3). Therefore, we assume that the erosion rates determined from the ^{10}Be concentrations reflect channel incision rates and can be used to calculate the erodibility K in equation (2).

Using k_{sn} and basin-averaged erosion rates, we determined the erodibility coefficient K for granitic and metamorphic rocks. These were 1.77×10^{-5} (n = 2/3), 4.85×10^{-6} (n = 1), and 3.70×10^{-7} (n = 5/3) m$^{0.1}$/yr for granitic rocks. To verify these estimates, we calculated erodibility coefficients for similar granitic rocks in the Abukuma massif (Kubo & Yamamoto, 1990) north of the study area using the same DEM and procedure we used in Iwaki (Figure S4; Tables S3, S4). We relied on ^{10}Be concentrations of fluvial sand reported by Regalla et al. (2013), Nakamura et al. (2014), and Matsushi et al. (2014) to recalculate basin-averaged erosion rates using the same method used in Iwaki. The resulting erodibility coefficients were similar to those obtained in Iwaki: 1.58×10^{-5} (n = 2/3), 4.52×10^{-6} (n = 1), and 3.90×10^{-7} (n = 5/3) m$^{0.1}$/yr. The coefficients for metamorphic rocks in Iwaki were 1.64×10^{-5} (n = 2/3), 5.21×10^{-6} (n = 1), and 5.30×10^{-7} (n = 5/3) m$^{0.1}$/yr, which were not very different from those for granitic rocks. Although sample limitations may affect the accuracy of the coefficient for metamorphic rocks, considering that the reaches of granitic and metamorphic rocks have comparable channel steepness (Figure 1b), our results indicate that these two rock types have similar erodibility.

4.3. Knickpoint Travel Time

To estimate knickpoint travel time, we first calculated uplift (erosion) rates at the initial and final steady states, using equation (6), based on the standard detachment limited model of equation (3) (Table 3). Given the erosion rates derived from ^{10}Be data (Table 2), a slope exponent of n = 2/3 yields the most probable estimates of initial and final uplift rates (Table 3). When calculating knickpoint travel time, we assumed that knickpoints were generated where the stream intersects the Yunodake fault. The resulting knickpoint travel times were somewhat similar among Basins 3−6, while the travel time for Basin 1 was much longer than those for the other basins (Table 4).

Table 2

Basin-averaged Erosion Rates Determined from ^{10}Be Concentrations

Sample ID	Mass sample (g)	Mass ^{9}Be carrier (g)	^{10}Be/^{9}Be ($\times10^{-14}$)[a]	^{10}Be concentration (atoms/g)	^{10}Be production rate (atoms/g yr)[b]	Erosion rate (g/m^{2}yr)	Erosion rate (mm/yr)[c]	Upstream ave. k_{sn} (m$^{0.9}$)[d]
IWK1	26.4364	3.4882	7.5 ± 0.51	55627 ± 4929	7.0 ± 0.4	261 ± 37	0.16 ± 0.03	28
IWK4	39.3525	2.4981	17.5 ± 2.2	67402 ± 9578	6.6 ± 0.4	391 ± 63	0.24 ± 0.04	59
IWK3	39.4954	2.4994	10 ± 0.90	34884 ± 4041	7.2 ± 0.4	405 ± 62	0.25 ± 0.04	25
IWK4-2	40.0002	2.4809	10.6 ± 0.88	36878 ± 3920	6.9 ± 0.4	329 ± 46	0.20 ± 0.03	17
IWK4-1*						444 ± 78	0.28 ± 0.05	90

Note. * Average rate for the downstream sub-catchment of Basin 4 calculated from equation (10).

[a] Results based on the KNB5-1 ^{10}Be standard (Nishiizumi et al., 2007). The ^{10}Be/^{9}Be ratio for the chemical blank was $1.8\times10^{-14} \pm 0.30\times10^{-14}$.

[b] We used the production rate at sea level and high latitude of 4.68 atoms g^{-1} yr^{-1}, corrected from the value proposed by Stone (2000) assuming a ^{10}Be half-life of 1.387 My (Chmeleff et al., 2010; Korschinek et al., 2010).

[c] The bulk density of samples was 1.63 g/cm^3 (Nakamura et al., 2014).

[d] Average k_{sn} for trunk and tributaries upstream from a sampling point.

Table 3

Initial and Final Uplift Rates Used to Calculate Knickpoint Travel Time

			n = 2/3		n = 1		n = 5/3	
Basin	$k_{sn\ ini}$	$k_{sn\ fin}$	U_{ini} (mm/yr)	U_{fin} (mm/yr)	U_{ini} (mm/yr)	U_{fin} (mm/yr)	U_{ini} (mm/yr)	U_{fin} (mm/yr)
2	15.1	61.7	0.10	0.26	0.08	0.32	0.05	0.51

3	31	120	0.17	0.40	0.15	0.63	0.11	1.54
4	20.5	122.4	0.13	0.44	0.10	0.59	0.06	1.12
5	57.2	87.9	0.26	0.35	0.28	0.43	0.31	0.64
6	12	94	0.09	0.37	0.06	0.46	0.02	0.72

Note. Uplift rates were calculated using normalized channel steepness and ^{10}Be analyses.

Table 4
Knickpoint Travel Time

Basin	Knickpoint position (m)	Travel time, n = 2/3 (My)	Travel time, n = 1 (My)	Travel time, n = 5/3 (My)
2	3908	0.73	1.38	2.16
3	2896	0.28	0.45	0.93
4	1154	0.21	0.42	0.69
5	1933	0.40	0.53	0.98
6	2550	0.28	0.62	0.97

4.4. Adjustment Timescales

The delay times for hillslope angle ranged between 0 and 0.3 My and were much shorter than those for channel width (Figure 8). The response times, too, were shorter for hillslope angle than for channel width. The most preferred case (n = 2/3) predicted that the change in hillslope angle was finished within 5-230 ky after the knickpoint passage. This result is consistent with response timescales reported in the Oregon Coast Range (Roering et al., 2001) and the Feather River basin, California (Hurst et al., 2012), which were estimated from sediment transport laws. The adjustment time for channel width was 2–5 times longer than those of hillslope angles.

While it is relatively easy to classify hillslopes into sections based on their degree of adjustment to the new boundary conditions (Figures 2 and 7), doing the same for channel width is tricky (Figures 4 and 7). One reason is the large variability in channel width (Figure 4); another is the large uncertainty in determining when an adjusting channel has achieved the steady-state form predicted by equation (4). Although we determined that the most downstream sections in Basins 3, 5, and 6 have adjusted to accelerated incision, it is also possible that our interpretation is wrong. Therefore, the response and adjustment times of channel width shown in Figure 8 are minimum estimates.

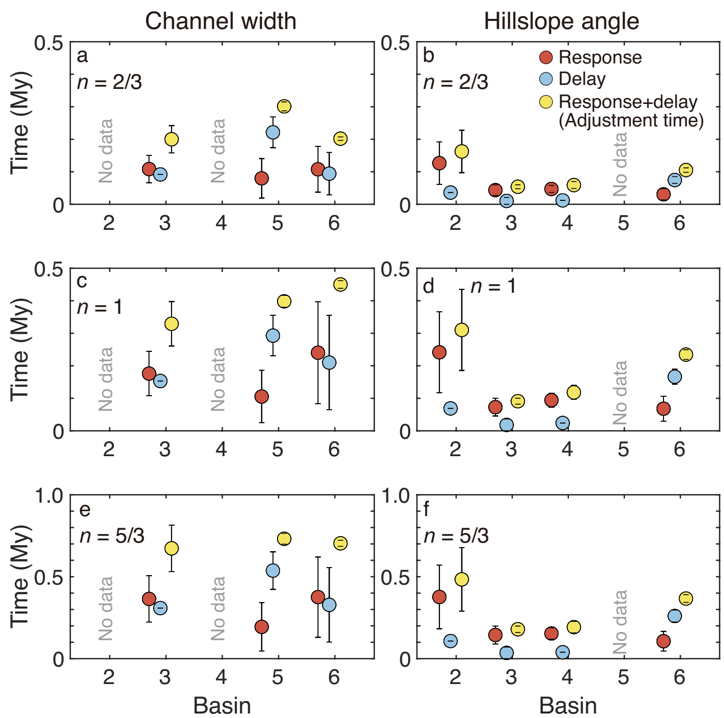

Figure 8. Delay, response, and adjustment times of channel width (a–c) and hillslope angle (d–f) in response to an increase in incision rates for three different values of *n*.

5. Discussion

5.1. Cause of Knickpoint Formation

The common occurrence of slope-break knickpoints and the similar erodibility coefficients between granitic and metamorphic rocks suggest that incision rates have increased in the study area. The average erosion rates in Basin 3, which are different upstream and downstream of the slope-break knickpoint, support the idea that accelerated river incision is responsible for the observed transient behavior.

We interpret the increase in incision rates to the activity of the Yunodake fault because rivers flowing across the fault (Basins 2–6) are much steeper than the river in Basin 1, away from the fault (Figure 1). Awata and Kakimi (1985) and Awata (1988) estimated initiation ages of active faulting in the current stress regime on the Pacific side of Tohoku on the basis of average slip rates and cumulative displacement. They found that many faults became active after 0.5–1.0 Ma. Doke et al. (2012) conducted an extensive literature review and reached a similar conclusion. Our modeled knickpoint travel times in Iwaki (Table 4) ranged between 0.2 and 0.7 My, consistent with the inferred onset of fault activity in Tohoku. Therefore, although there is no direct evidence of the throw rate of the Yunodake fault increasing during the middle Pleistocene, we attribute the generation of slope-break knickpoints to changes in throw rates of the fault.

5.2. Implications for Transient Response

The delay and response times of channel width are 2–5 times longer than those of hillslope angle. Depending on the erosion process (the slope exponent n in equation (2)) and the magnitude of the acceleration of river incision, width adjustment can take 0.16–0.81 My after the knickpoint passage (Figure 8). In addition, our observations confirmed that the transient response takes place at different spatiotemporal scales for channel slope, channel width, and hillslope angle. Thus channel width and hillslope angle may be continuing to adjust even when the river lacks a prominent knickpoint. Since channel characteristics and hillslope morphology are the primary controls of river incision (e.g., Whipple & Tucker, 2002), correctly identifying the adjusted sections within a catchment is essential for assessing the transient response to an increase in incision rates.

Another inference from our observation is on the transient response of channel width. The ratio of sediment supply to transport capacity dictates the dynamics of channel width adjustment (e.g., Finnegan et al., 2007; Yanites & Tucker, 2010; Baynes et al., 2020). Because the total sediment supply into a channel is modulated by the form of upstream hillslopes (e.g., Roering et al., 2007), the adjustment of channel width is expected to continue until a slope-break knickpoint reaches the headwaters and adjacent hillslopes achieve their steady-state forms. However, despite the fact that most hillslopes exhibit pre-adjustment forms in Basins 3, 5, and 6 (Figures 6b and 6c), the channel widths in their downstream sections appear to be adjusted to the accelerated incision (Figures 4 and S5, Table S4). It appears, then, that the dynamics of width adjustment are not simply a response to the increase in total sediment supply from upstream.

An alternative interpretation is that the channel width adjustment has not in fact been completed, and the ongoing changes in the channel are too small to be confidently detected due to measurement error and natural variability. This interpretation is compatible with the result of numerical modeling, which predicts that the response of channel width is rapid at first, then decays as the response progresses (Yanites, 2018). We speculate that this gradual decrease is related to the downstream fining of sediment. Abrasion and selective transport are the main drivers of downstream fining (i.e., mass reduction) of sediment (e.g., Parker, 1991). Their effects typically scale with travel distance and can be significant even after only a few kilometers of transport (e.g., Parker, 1991; Phillips & Jerolmack, 2014; Miller et al., 2014). Therefore, the rate of increase in sediment supply at a point downstream should slow as the knickpoint travels upstream, as demonstrated by numerical experiments (Yanites, 2018). Given the dependence of channel width on grain size and the ratio of sediment supply to transport capacity (e.g., Yanites & Tucker, 2010; Finnegan et al., 2017), we attribute the decay in the response speed of channel width to a decline in the rate of increase in sediment supply.

5.3. Timescale of Catchment-Scale Adjustment

The adjustment of an entire catchment is a more complex matter than the adjustment of a trunk stream. Knickpoint travel speed depends on stream discharge (e.g., Whipple & Tucker, 1999; Hayakawa & Matsukura, 2003; Bishop et al., 2005), and the travel time from its origin to the channel head is on the order of 10^5–10^6 years (Whipple, 2001; Whittaker and Boulton, 2012). The adjustment of channel slopes in tributaries must also be considered; this is sometimes prolonged where hanging valleys are present (Wobus et al., 2006b; Crosby et al., 2007; DiBiase et al., 2015). Adjustments of channel width and hillslope require hundreds of thousands more years after a knickpoint has finished propagating to the heads of the trunk and tributaries. Moreover, other aspects of channels and hillslopes respond to changes in channel incision rates, such as channel sinuosity (Turowski, 2018) and hilltop curvature (Gabet et al., 2021). Morphological adjustments of these variables are also triggered by climate variability and occur at timescales of 10^5–10^6 years (e.g., Whipple, 2001), although fluvial systems might not fully adjust to high-frequency climatic oscillations such as Milankovitch cycles (Armitage et al., 2013; Goren, 2016). Given all these factors, it is clear that catchment-scale adjustment to accelerated incision takes much longer than the knickpoint travel time within the trunk stream. This further confirms that to estimate rates of erosion or base-level fall, one must consider whether the river system has reached a steady state even when it contains no prominent knickpoint.

6. Conclusions

Based on the observed channel and hillslope geometries and knickpoint travel time, we have estimated their adjustment times to accelerated incision. Our approach enables us to estimate both delay and response times of channel width and hillslope angles, which are otherwise difficult to constrain in an actual landscape. Our results indicate that hillslope adjustment starts and finishes much earlier than channel width adjustment. Change in hillslope angle starts soon after the passage of a knickpoint (10^0–10^4 yr) and generally finishes on the order of 10^5 years later. Channel width adjustment takes 2–5 times longer than hillslope adjustment. Unlike hillslope angle, channel width has adjustment times that are not always negligible compared to that of channel slope, which depends closely on knickpoint travel time.

The longevity of catchment-scale adjustment time and the different adjustment timescales among channel slope, channel width, and hillslope angles remind us that we need to infer erosion or uplift rates from channel reaches that are in a well-defined steady state. Our findings also suggest that it is important to understand the temporal evolution of erosion rates during the adjustment of individual channel and hillslope components. Lastly, it has to be noted that our estimates of knickpoint travel time do not explicitly consider important factors including the effects of sediment characteristics and temporal changes in precipitation. Because these factors may significantly alter estimates of adjustment time, inter-model comparisons or more sophisticated models of migrating knickpoints are necessary to better understand the transient response of bedrock rivers.

Acknowledgments

We thank Chia-Yu Chen (National Taiwan University) for helpful comments and A. Morikawa, K. Kitamura (Kyoto University), N. Miyauchi, and Y. Tsuchiya (The University of Tokyo) for their assistance during preparation of the ^{10}Be samples. This work was supported by the International Joint Graduate Program in Earth and Environmental Sciences, Tohoku University. N. Takahashi and R. Ohta thank the staff at Yunodake sanso in Iwaki for their generous support during our fieldwork. We obtained DEM data from the Geospatial Authority of Japan and NOAA (ETOPO1). Some color maps were obtained from Crameri (2018).

References

Ahnert, F. (1970). Functional relationships between denudation, relief, and uplift in large mid-latitude drainage basins. *American Journal of science*, 268, 243–263. https://doi.org/10.2475/ajs.268.3.243

Allen, G. H., Barnes, J. B., Pavelsky, T. M., & Kirby, E. (2013). Lithologic and tectonic controls on bedrock channel form at the northwest Himalayan front. *Journal of Geophysical Research: Earth Surface*, 118(3), 1806–1825. https://doi.org/10.1002/jgrf.20113

Armitage, J. J., Dunkley Jones, T., Duller, R. A., Whittaker, A. C., & Allen, P. A. (2013). Temporal buffering of climate-driven sediment flux cycles by transient catchment response. *Earth and Planetary Science Letters*, 369–370, 200–210. https://doi.org/10.1016/j.epsl.2013.03.020

Awata, Y. (1988). Shortening of the central inner arc of the northeast Japan and movement of the Pacific plate. *Chikyu Monthly*, 10(9), 586–591.

Awata, Y., & Kakimi, T. (1985). Quaternary tectonics and damaging earthquakes in northeast Honshu, Japan. *Earthquake Prediction Research*, 3, 231–251.

Baynes, E. R. C., Lague, D., Steer, P., Bonnet, S., & Illien, L. (2020). Sediment flux-driven channel geometry adjustment of bedrock and mixed gravel–bedrock rivers. *Earth Surface Processes and Landforms*, 45(14), 3714–3731. https://doi.org/10.1002/esp.4996

Baynes, E. R. C., Lague, D., Steer, P., & Davy, P. (2022). Dynamic bedrock channel width during knickpoint retreat enhances undercutting of coupled hillslopes. *Earth Surface Processes and Landforms*. https://doi.org/10.1002/esp.5477

Bierman, P., & Steig, E. J. (1996). Estimating rates of denudation using cosmogenic isotope abundances in sediment. *Earth Surface Processes and Landforms*, 21(2), 125–139. https://doi.org/10.1002/(sici)1096-9837(199602)21:2<125::aid-esp511>3.0.co;2-8

Bishop, P., Hoey, T. B., Jansen, J. D., & Lexartza Artza, I. (2005). Knickpoint recession rate and catchment area: The case of uplifted rivers in eastern Scotland. *Earth Surface Processes and Landforms*, 30(6), 767–778. https://doi.org/10.1002/esp.1191Braucher, R., Brown, E. T., Bourlès, D. L., & Colin, F. (2003). In situ produced ^{10}Be measurements at great depths: Implications for production rates by fast muons. *Earth and Planetary Science Letters*, 211(3–4), 251–258. https://doi.org/10.1016/S0012-821X(03)00205-X

Brown, E. T., Stallard, R. F., Larsen, M. C., Raisbeck, G. M., & Yiou, F. (1995a). Denudation rates determined from the accumulation of in situ-produced ^{10}Be in the luquillo experimental forest, Puerto Rico. *Earth and Planetary Science Letters*, 129(1–4), 193–202. https://doi.org/10.1016/0012-821X(94)00249-X

Brown, E. T., Bourlès, D. L., Colin, F., Raisbeck, G. M., Yiou, F., & Desgarceaux, S. (1995b). Evidence for muon-induced production of ^{10}Be in near-surface rocks from the Congo. *Geophysical Research Letters*, 22(6), 703-706. https://doi.org/10.1029/95GL00167

Chen, Y. W., Shyu, J. B. H., & Chang, C. P. (2015). Neotectonic characteristics along the eastern flank of the Central Range in the active Taiwan orogen inferred from fluvial channel morphology. *Tectonics*, 34(10), 2249–2270. https://doi.org/10.1002/2014TC003795

Chmeleff, J., von Blanckenburg, F., Kossert, K., & Jakob, D. (2010). Determination of the ^{10}Be half-life by multicollector ICP-MS and liquid scintillation counting. *Nuclear Instruments and Methods in Physics Research, Section B: Beam Interactions with Materials and Atoms*, 268(2), 192–199. https://doi.org/10.1016/j.nimb.2009.09.012

Crameri, F. (2018). Scientific colour maps (Version 7.0.0). *Zenodo*. https://doi.org/10.5281/ZENODO.1243862

Crosby, B. T., & Whipple, K. X. (2006). Knickpoint initiation and distribution within fluvial networks: 236 waterfalls in the Waipaoa River, North Island, New Zealand. *Geomorphology*, 82(1–2), 16–38. https://doi.org/10.1016/j.geomorph.2005.08.023

Crosby, B. T., Whipple, K. X., Gasparini, N. M., & Wobus, C. W. (2007). Formation of fluvial hanging valleys: Theory and simulation. *Journal of Geophysical Research*, 112(F3), F03S10. https://doi.org/10.1029/2006JF000566

DiBiase, R. A., Heimsath, A. M., & Whipple, K. X. (2012). Hillslope response to tectonic forcing in threshold landscapes. *Earth Surface Processes and Landforms*, 37(8), 855–865. https://doi.org/10.1002/esp.3205

DiBiase, R. A., Whipple, K. X., Lamb, M. P., & Heimsath, A. M. (2015). The role of waterfalls and knickzones in controlling the style and pace of landscape adjustment in the western San Gabriel Mountains, California. *Bulletin of the Geological Society of America*, 127(3–4), 539–559. https://doi.org/10.1130/B31113.1

Doke, R., Tanikawa, S., Yasue, K., Nakayasu, A., Niizato, T., Umeda, K., & Tanaka, T. (2012). Spatial patterns of initiation ages of active faulting in the Japanese islands. *Active Fault Research*, 37, 1–15. https://doi.org/10.11462/afr.2012.37_1

Finnegan, N. J., Sklar, L. S., & Fuller, T. K. (2007). Interplay of sediment supply, river incision, and channel morphology revealed by the transient evolution of an experimental bedrock channel. *Journal of Geophysical Research: Earth Surface*, 112(3), 1–17. https://doi.org/10.1029/2006JF000569

Finnegan, N. J., Klier, R. A., Johnstone, S., Pfeiffer, A. M., & Johnson, K. (2017). Field evidence for the control of grain size and sediment supply on steady-state bedrock river channel slopes in a tectonically active setting. *Earth Surface Processes and Landforms*, 42(14), 2338–2349. https://doi.org/10.1002/esp.4187

Flint, J. J. (1974). Stream gradient as a function of order, magnitude, and discharge. *Water Resources Research*, 10(5), 969–973. https://doi.org/10.1029/WR010i005p00969

Fukushima, Y., Takada, Y., & Hashimoto, M. (2013). Complex ruptures of the 11 April 2011 Mw 6.6 Iwaki earthquake triggered by the 11 March 2011 Mw 9.0 Tohoku earthquake, Japan. *Bulletin of the Seismological Society of America*, 103(2 B), 1572–1583. https://doi.org/10.1785/0120120140

Gabet, E. J., Mudd, S. M., Wood, R. W., Grieve, S. W. D., Binnie, S. A., & Dunai, T. J. (2021). Hilltop curvature increases with the square root of erosion rate. *Journal of Geophysical Research: Earth Surface*, 126(5), 1–16. https://doi.org/10.1029/2020jf005858

Gallen, S. F., & Wegmann, K. W. (2017). River profile response to normal fault growth and linkage: An example from the Hellenic forearc of south-central Crete, Greece. *Earth Surface Dynamics*, 5(1), 161–186. https://doi.org/10.5194/esurf-5-161-2017

Geological Survey of Japan, 2020. Seamless Digital Geological Map of Japan. Geological Survey of Japan. Retrieved from https://gbank.gsj.jp/seamless/v2.html

Goren, L. (2016). A theoretical model for fluvial channel response time during time-dependent climatic and tectonic forcing and its inverse applications. *Geophysical Research Letters*, 43(20), 10,753-10,763. https://doi.org/10.1002/2016GL070451

Gosse, J. C., & Phillips, F. M. (2001). Terrestrial in situ cosmogenic nuclides: Theory and application. *Quaternary Science Reviews*, 20(14), 1475–1560. https://doi.org/10.1016/S0277-3791(00)00171-2

Granger, D. E., Kirchner, J. W., & Finkel, R. (1996). Spatially averaged long-term erosion rates measured from in situ-produced cosmogenic nuclides in alluvial sediment. *Journal of Geology*, 104(3), 249–257. https://doi.org/10.1086/629823

Hayakawa, Y., & Matsukura, Y. (2003). Recession rates of waterfalls in Boso Peninsula, Japan, and a predictive equation. *Earth Surface Processes and Landforms*, 28(6), 675–684. https://doi.org/10.1002/esp.519

Hiroi, Y., Yokose, M., Oba, T., Kishi, S., Nohara, T., & Yao, A. (1987). Discovery of Jurassic radiolaria from acmite-rhodonite-bearing metachert of the Gosaisyo metamorphic rocks in the Abukuma terrane, northeastern Japan. *Journal of the Geological Society of Japan*, 93(6), 445–448. https://doi.org/10.5575/geosoc.93.445

Howard, A. D., & Kerby, G. (1983). Channel changes in badlands. *Geological Society of America Bulletin*, 94(6), 739–752. https://doi.org/10.1130/0016-7606(1983)94<739:CCIB>2.0.CO;2

Hurst, M. D., Mudd, S. M., Walcott, R., Attal, M., & Yoo, K. (2012). Using hilltop curvature to derive the spatial distribution of erosion rates. *Journal of Geophysical Research: Earth Surface*, 117(F2), F02017. https://doi.org/10.1029/2011JF002057

Imanishi, K., Ando, R., & Kuwahara, Y. (2012). Unusual shallow normal-faulting earthquake sequence in compressional northeast Japan activated after the 2011 off the Pacific coast of Tohoku earthquake. *Geophysical Research Letters*, 39(9), L09306. https://doi.org/10.1029/2012GL051491

Japan Meteorological Agency (2021). Past meteorological data. http://www.data.jma.go.jp/obd/stats/etrn/index.php (accessed 27 April, 2021)

Kano, H., Kuroda, Y., Uruno, K., Nureki, T., Kanisawa, S., Maruyama, T., Umemura, H., Matsukawa, H., Seto, N., Ohira, Y., Sato, S., & Isshiki, N. (1973). Geology of the Takanuki district (07-70, scale 1:50,000). Tsukuba: Geological Survey of Japan.Kirby, E., & Whipple, K. X. (2012). Expression of active tectonics in erosional landscapes. *Journal of Structural Geology*, 44, 54–75. https://doi.org/10.1016/j.jsg.2012.07.009

Kohl, C., & Nishiizumi, K. (1992). Chemical isolation of quartz for measurement of in-situ-produced cosmogenic nuclides. *Geochimica et Cosmochimica Acta*, 56(9), 3583–3587. https://doi.org/10.1016/0016-7037(92)90401-4

Korschinek, G., Bergmaier, A., Faestermann, T., Gerstmann, U. C., Knie, K., Rugel, G., et al. (2010). A new value for the half-life of ^{10}Be by Heavy-Ion Elastic Recoil Detection and liquid scintillation counting. *Nuclear Instruments and Methods in Physics Research, Section B: Beam Interactions with Materials and Atoms*, 268(2), 187–191.

https://doi.org/10.1016/j.nimb.2009.09.020

Kubo, K., & Yamamoto, T. (1990). Cretaceous intrusive rocks of the Haramachi district, eastern margin of the Abukuma mountains. *Journal of Geological Society of Japan*, 96(9), 731–743. https://doi.org/10.5575/geosoc.96.731

Kubo, K., Yanagisawa, Y., Yamamoto, T., Nakae, S., Takahashi, Y., Toshimitsu, S., Banno, Y., Miyachi, Y., Takahashi, M., Komazawa, M., & Ohno, T. (2007). Geological map of Japan, Shirakawa (NJ54-17·23, scale 1:200,000). Tsukuba: Geological Survey of Japan.

Lavé, J., & Avouac, J. P. (2001). Fluvial incision and tectonic uplift across the Himalayas of central Nepal. *Journal of Geophysical Research: Solid Earth*, 106(B11), 26561–26591. https://doi.org/10.1029/2001jb000359

Li, Y.-k. (2013). Determining topographic shielding from digital elevation models for cosmogenic nuclide analysis: A GIS approach and field validation. *Journal of Mountain Science*, *10*(3), 355–362. https://doi.org/10.1007/s11629-013-2564-1

Matsushi, Y., Matsuzaki, H., & Makino, H. (2014). Testing models of landform evolution by determining the denudation rates of mountains watersheds using terrestrial cosmogenic nuclides. *Transactions, Japanese Geomorphological Union*, 35(2), 165–185.

Matsuzaki, H., Nakano, C., Tsuchiya, Y. (Sunohara), Kato, K., Maejima, Y., Miyairi, Y., et al. (2007). Multi-nuclide AMS performances at MALT. *Nuclear Instruments and Methods in Physics Research, Section B: Beam Interactions with Materials and Atoms*, 259(1), 36–40. https://doi.org/10.1016/j.nimb.2007.01.145

Miller, K. L., Szabó, T., Jerolmack, D. J., & Domokos, G. (2014). Quantifying the significance of abrasion and selective transport for downstream fluvial grain size evolution. *Journal of Geophysical Research: Earth Surface*, 119(11), 2412–2429. https://doi.org/10.1002/2014JF003156

Mitchell, N. A., & Yanites, B. J. (2019). Spatially variable increase in rock uplift in the northern U.S. Cordillera recorded in the distribution of river knickpoints and incision depths. *Journal of Geophysical Research: Earth Surface*, 124(5), 1238–1260. https://doi.org/10.1029/2018JF004880

Mitsui, S. (1971). Studies on the mechanism of deformation of sedimentary rocks in the Iwaki area of the Joban Coal-Field, Fukushima Prefecture. *The science reports of the Tohoku University. Second series, Geology*, 42, 199–272. http://hdl.handle.net/10097/28814

Miyashita, Y. (2018). Holocene paleoseismic history of the Yunodake fault ruptured by the 2011 Fukushima-ken Hamadori earthquake, Fukushima Prefecture, Japan. *Geomorphology*, 323, 70–79. https://doi.org/10.1016/j.geomorph.2018.08.040

Montgomery, D. R., & Brandon, M. T. (2002). Topographic controls on erosion rates in tectonically active mountain ranges. *Earth and Planetary Science Letters*, 201(3–4), 481–489. https://doi.org/10.1016/S0012-821X(02)00725-2

Montgomery, D. R., & Foufoula-Georgiou, E. (1993). Channel network source representation using digital elevation models. *Water Resources Research*, 29(12), 3925–3934. https://doi.org/10.1029/93WR02463

Montgomery, D. R., & Gran, K. B. (2001). Downstream variations in the width of bedrock channels. *Water Resources Research*, 37(6), 1841–1846. https://doi.org/10.1029/2000WR900393

Mudd, S. M., & Furbish, D. J. (2007). Responses of soil-mantled hillslopes to transient channel incision rates. *Journal of Geophysical Research: Earth Surface*, 112(3), 1–12. https://doi.org/10.1029/2006JF000516

Nakamura, A., Yokoyama, Y., Shiroya, K., Miyairi, Y., & Matsuzaki, H. (2014). Direct comparison of site-specific and basin-scale denudation rate estimation by in situ cosmogenic nuclides: An example from the Abukuma Mountains, Japan. *Progress in Earth and Planetary Science*, 1(1), 1–11. https://doi.org/10.1186/2197-4284-1-9

Nakata, T., & Imaizumi, T. (Eds.) (2002). Digital active fault map of Japan. Tokyo: University of Tokyo press.

Nishiizumi, K., Imamura, M., Caffee, M. W., Southon, J. R., Finkel, R. C., & McAninch, J. (2007). Absolute calibration of ^{10}Be AMS standards. *Nuclear Instruments and Methods in Physics Research, Section B: Beam Interactions with Materials and Atoms*, 258(2), 403–413. https://doi.org/10.1016/j.nimb.2007.01.297

Ouimet, W. B., Whipple, K. X., & Granger, D. E. (2009). Beyond threshold hillslopes: Channel adjustment to base-level fall in tectonically active mountain ranges. *Geology*, 37(7), 579–582. https://doi.org/10.1130/G30013A.1

Parker, G. (1991). Selective sorting and abrasion of river gravel. I: Theory. *Journal of Hydraulic Engineering*, 117(2), 131–147. https://doi.org/10.1061/(ASCE)0733-9429(1991)117:2(131)

Perron, J. T., & Royden, L. (2013). An integral approach to bedrock river profile analysis. *Earth Surface Processes and Landforms*, 38(6), 570–576. https://doi.org/10.1002/esp.3302

Phillips, C. B., & Jerolmack, D. J. (2014). Dynamics and mechanics of bed-load tracer particles. *Earth Surface Dynamics*, 2(2), 513–530. https://doi.org/10.5194/esurf-2-513-2014

Regalla, C., Kirby, E., Fisher, D., & Bierman, P. (2013). Active forearc shortening in Tohoku, Japan: Constraints on fault geometry from erosion rates and fluvial longitudinal profiles. *Geomorphology*, 195, 84–98. https://doi.org/10.1016/j.geomorph.2013.04.029

Reinhardt, L. J., Bishop, P., Hoey, T. B., Dempster, T. J., & Sanderson, D. C. W. (2007). Quantification of the transient response to base-level fall in a small mountain catchment: Sierra Nevada, southern Spain. *Journal of Geophysical Research*, 112(F3), F03S05. https://doi.org/10.1029/2006JF000524

Roering, J. J. (2008). How well can hillslope evolution models “explain” topography? Simulating soil transport and production with high-resolution topographic data. *Bulletin of the Geological Society of America*, 120(9–10), 1248–1262. https://doi.org/10.1130/B26283.1

Roering, J. J., Kirchner, J. W., & Dietrich, W. E. (2001). Hillslope evolution by nonlinear, slope-dependent transport: Steady state morphology and equilibrium adjustment timescales. *Journal of Geophysical Research: Solid Earth*, 106(B8), 16499–16513. https://doi.org/10.1029/2001jb000323

Roering, J. J., Perron, J. T., & Kirchner, J. W. (2007). Functional relationships between denudation and hillslope form and relief. *Earth and Planetary Science Letters*, 264(1–2), 245–258. https://doi.org/10.1016/j.epsl.2007.09.035

Royden, L., & Perron, J. T. (2013). Solutions of the stream power equation and application to the evolution of river longitudinal profiles. *Journal of Geophysical Research: Earth Surface*, 118(2), 497–518. https://doi.org/10.1002/jgrf.20031

Schwanghart, W., & Scherler, D. (2014). Short Communication: TopoToolbox 2 - MATLAB-based software for topographic analysis and modeling in Earth surface sciences. *Earth Surface Dynamics*, 2(1), 1–7. https://doi.org/10.5194/esurf-2-1-2014

Snyder, N. P., Whipple, K. X., Tucker, G. E., & Merritts, D. J. (2000). Landscape response to tectonic forcing: Digital elevation model analysis of stream profiles in the Mendocino triple junction region, Northern California. *Bulletin of the Geological Society of America*, 112(8), 1250–1263. https://doi.org/10.1130/0016-7606(2000)112<1250:LRTTFD>2.0.CO;2

Snyder, N. P., Whipple, K. X., Tucker, G. E., & Merritts, D. J. (2003). Channel response to tectonic forcing: Field analysis of stream morphology and hydrology in the Mendocino triple junction region, northern California. *Geomorphology*, 53(1–2), 97–127. https://doi.org/10.1016/S0169-555X(02)00349-5

Stock, J., & Dietrich, W. E. (2003). Valley incision by debris flows: Evidence of a topographic signature. *Water Resources Research*, 39(4), 1089. https://doi.org/10.1029/2001WR001057

Stone, J. O. (2000). Air pressure and cosmogenic isotope production. *Journal of Geophysical Research*, 105(B10), 23753–23759. https://doi.org/10.1029/2000jb900181

Toda, S., & Tsutsumi, H. (2013). Simultaneous reactivation of two, subparallel, inland normal faults during the Mw 6.6 11 April 2011 Iwaki earthquake triggered by the M w 9.0 Tohoku-oki, Japan, Earthquake. *Bulletin of the Seismological Society of America*, 103(2 B), 1584–1602. https://doi.org/10.1785/0120120281

Turowski, J. M. (2018). Alluvial cover controlling the width, slope and sinuosity of bedrock channels. *Earth Surface Dynamics*, 6(1), 29–48. https://doi.org/10.5194/esurf-6-29-2018

Turowski, J. M. (2020). Mass balance, grade, and adjustment timescales in bedrock channels. *Earth Surface Dynamics*, 8(1), 103–122. https://doi.org/10.5194/esurf-8-103-2020

Whipple, K. X. (2001). Fluvial Landscape Response Time: How Plausible Is Steady-State Denudation? *American Journal of Science*, 301(4–5), 313–325. https://doi.org/10.2475/ajs.301.4-5.313

Whipple, K. X. (2004). Bedrock rivers and the geomorphology of active orogens. *Annual Review of Earth and Planetary Sciences*, 32(1), 151–185. https://doi.org/10.1146/annurev.earth.32.101802.120356

Whipple, K. X., & Tucker, G. E. (1999). Dynamics of the stream-power river incision model: Implications for height limits of mountain ranges, landscape response timescales, and research needs. *Journal of Geophysical Research: Solid Earth*, 104(B8), 17661–17674. https://doi.org/10.1029/1999jb900120

Whipple, K. X., & Tucker, G. E. (2002). Implications of sediment-flux-dependent river incision models for landscape evolution. *Journal of Geophysical Research*, 107(B2), 2039.

https://doi.org/10.1029/2000jb000044

Whipple, K. X., Hancock, G. S., & Anderson, R. S. (2000). River incision into bedrock: Mechanics and relative efficacy of plucking, abrasion, and cavitation. *Bulletin of the Geological Society of America*, 112(3), 490–503. https://doi.org/10.1130/0016-7606(2000)112<490:RIIBMA>2.0.CO;2

Whipple, K. X, DiBiase, R. A., & Crosby, B. T. (2013). Bedrock rivers. In Shroder, J. (Editor in Chief), Wohl, E. (Ed.), *Treatise on Geomorphology* (Vol. 9, pp. 550–573). San Diego, CA: Academic Press. https://doi.org/10.1016/B978-0-12-374739-6.00254-2

Whittaker, A. C., & Boulton, S. J. (2012). Tectonic and climatic controls on knickpoint retreat rates and landscape response times. *Journal of Geophysical Research: Earth Surface*, 117(F2), F02024. https://doi.org/10.1029/2011JF002157

Whittaker, A. C., Cowie, P. A., Attal, M., Tucker, G. E., & Roberts, G. P. (2007). Contrasting transient and steady-state rivers crossing active normal faults: New field observations from the Central Apennines, Italy. *Basin Research*, 19(4), 529–556. https://doi.org/10.1111/j.1365-2117.2007.00337.x

Wobus, C. W., Whipple, K. X., Kirby, E., Snyder, N., Johnson, J., Spyropolou, K., et al. (2006a). Tectonics from topography: Procedures, promise, and pitfalls. In Special Paper 398: Tectonics, Climate, and Landscape Evolution (Vol. 398, pp. 55–74). https://doi.org/10.1130/2006.2398(04)

Wobus, C. W., Crosby, B. T., & Whipple, K. X. (2006b). Hanging valleys in fluvial systems: Controls on occurrence and implications for landscape evolution. *Journal of Geophysical Research: Earth Surface*, 111(2), F02017. https://doi.org/10.1029/2005JF000406

Yanites, B. J. (2018). The dynamics of channel slope, width, and sediment in actively eroding bedrock river systems. *Journal of Geophysical Research: Earth Surface*, 123(7), 1504–1527. https://doi.org/10.1029/2017JF004405

Yanites, B. J., & Tucker, G. E. (2010). Controls and limits on bedrock channel geometry. *Journal of Geophysical Research*, 115(F4), F04019. https://doi.org/10.1029/2009JF001601

Zhang, H., Kirby, E., Pitlick, J., Anderson, R. S., & Zhang, P. (2017). Characterizing the transient geomorphic response to base-level fall in the northeastern Tibetan Plateau. *Journal of Geophysical Research: Earth Surface*, 122(2), 546–572. https://doi.org/10.1002/2015JF003715